Signal, Image and Video Processing (2026) 20:696
https://doi.org/10.1007/s11760-026-05559-0

ORIGINAL PAPER

A multi-model deep learning approach to detect tumors on Mohs micrographic surgery slides

Abdurrahim Yilmaz[1,2] · Serra Atilla Aydin[3,4] · Deniz Temur[2] · Furkan Yuceyalcin[2] · Berkin Deniz Kahya[2] · Rahmetullah Varol[2] · Ozay Gokoz[3] · Gulsum Gencoglan[5] · Huseyin Uvet[2] · Gonca Elcin[3]

Received: 20 March 2026 / Revised: 19 June 2026 / Accepted: 4 July 2026 / Published online: 14 October 2026
© The Author(s) 2026

Abstract

Mohs micrographic surgery (MMS) is the goldstandard technique for removing high-risk nonmelanoma skin cancers (NMSC); however, intraoperative histopathological examination requires significant time, effort, and specialist expertise. The objective of this study was to develop a deep learning model to detect basal cell carcinoma (BCC) and artifacts on Mohs slides. The objective of this study was to develop a deep learning model to detect basal cell carcinoma (BCC) and artifacts on Mohs slides. A total of 731 Mohs slides from 51 patients with BCC were used in this study, of which 91 contained tumor and 640 were classified as artifact. The dataset was used to train U-Net-based models to segment tumor and non-tumor regions on the slides. The segmented patches were classified as tumor or non-tumor to generate predictions for wholeslide images (WSIs). During segmentation, the tumor and artifact models achieved Dice scores of 0.70 and 0.67 and area under the curve (AUC) values of 0.98 and 0.96, respectively. For tumor classification, the patch-level and slide-level AUCs on the test set were 0.98 and 0.91, respectively. We present an AI system that can detect tumor and artifact regions in Mohs slides with promising performance. Deep learning can aid Mohs surgeons and dermatopathologists in making more accurate decisions.

Keywords Mohs micrographic surgery · Deep learning · Basal cell carcinoma · Histopathology

1 Introduction

Mohs micrographic surgery (MMS) is a precision-driven technique for treating non-melanoma skin cancers (NMSC). It employs a cyclic approach that begins with a minimal tumor excision followed by the mapping of the excised tissue and immediate intraoperative microscopic examination of the surgical margins. If remnant tumors are identified, additional excisions are carried out at the exact locations, as dictated by the map. This process repeats until all margins are clear of tumor cells, ensuring total eradication of the tumor while preserving as much healthy tissue as possible. The technique is not primarily a histopathological diagnostic tool for classifying skin tumors; rather, its value lies in identifying residual tumor at surgical margins, thereby reducing the risk of recurrence. Particularly effective for high-risk basal cell carcinoma (BCC), one of the most common cancers worldwide, MMS has become a gold-standard treatment.

However, a critical factor that determines the success of MMS is the intraoperative histopathological examination, which is labor-intensive and time-consuming. This drawback can impede the broader adoption of MMS, potentially affecting patient outcomes. The rapid development of machine learning technology holds promise in streamlining the demanding tasks, including the microscopic examination of Mohs slides. Deep learning, a subfield of machine learning, has shown remarkable capabilities in histopathological image analysis, thereby offering prospects of automation and

✉ Abdurrahim Yilmaz
a.yilmaz23@imperial.ac.uk

✉ Gonca Elcin
goncaelcin@gmail.com

1 Department of Metabolism, Digestion and Reproduction, Imperial College London, Burlington Danes, Du Cane Rd, W12 0TN London, United Kingdom

2 Mechatronics Engineering Department, Yildiz Technical University, Istanbul 34349, Turkey

3 Department of Dermatology, Hacettepe University, Ankara 06230, Turkey

4 Department of Dermatology, Venereology and Allergology, Charité Universitaetsmedizin Berlin, Berlin, Germany

5 Department of Dermatology, Istinye University, Istanbul 34408, Turkey

enhanced diagnostic and prognostic precision. Convolutional neural networks (CNNs), for instance, have demonstrated proficiency in tasks such as tumor detection, segmentation, and classification [1, 2]. Moreover, recent strides in transfer learning have allowed for the successful adaptation of pretrained models to dermatology, resulting in better performance and expedited training times [3, 4]. Generative models, such as generative adversarial networks (GANs), have also been used to mitigate limitations associated with small labeled datasets in histopathology through data augmentation and image synthesis [5].

In spite of these advancements, existing literature on tumor and non-tumor area detection in MMS is sparse. Zon et al. pioneered a patch-based segmentation model using 171 slides from 70 patients, which achieved an area under the curve (AUC) value of 0.90 for slide-level classification of BCC [6]. Nevertheless, the study was limited by reliance on a single expert for labeling and by limited detail regarding the statistical analysis. Similarly, Sohn et al. conducted a study that yielded an AUC of 0.75, but it was hindered by the use of a relatively small dataset [7]. Thus, there is a need for a more comprehensive dataset annotated in consensus by experts to support the robustness of the resulting algorithm. Moreover, it is becoming increasingly clear that the development of robust and reliable AI systems can help alleviate the burden on experts and provide swift feedback for surgical procedures.

In light of these considerations, this study aimed to develop an AI model capable of detecting tumor and artifact regions during the histopathological examination of MMS using a multi-model approach. We leveraged U-Net based deep learning models, known for their precision, to detect tumor and non-tumor regions in MMS images. We trained these models using 731 high-resolution MMS slides, including 91 tumor-positive and 640 artifact (tumor-negative) slides. Additionally, we computed specific metrics to assess the model's performance and reliability. The overarching intent of this study is to cultivate a synergy between human expertise and AI in histopathology to optimize the benefits and efficiency of MMS.

2 Methods

The dataset used in this retrospective study comprised hematoxylin and eosin (H&E)-stained histopathological slides obtained during MMS procedures performed between 2013 and 2020 in the MMS Unit of the Department of Dermatology, Hacettepe University Faculty of Medicine, by an ESMS-certified Mohs surgeon (G.E.). Mohs slides were stored in the archives of the Department of Pathology, all of which underwent routine intraoperative quality assessment by the reporting dermatopathologist (O.G.) to ensure suitability for complete surgical margin evaluation. For AI model development, slides with variable quality and pronounced artifacts were intentionally retained to increase model robustness, provided that tissue structures and annotated regions were sufficiently visible for expert annotation and digital processing. Slides were considered unsuitable only when image clarity, scanning quality, or tissue visualization was inadequate for reliable annotation or model training. Thus, the necessary standards referred to technical suitability for digital image analysis rather than the absence of artifacts. These H&E-stained frozen-section slides obtained during MMS were digitized using an Olympus VS120 digital slide scanner at $\times 40$ magnification, anonymized, and saved in .vsi format (S.A.). A total of 731 high-resolution whole-slide images from 51 patients were included. The authors (A.Y., D.T., F.Y., B.D.K., and R.V.) manually reviewed all slides in the dataset to ensure that they met the necessary standards, such as adequate image clarity, for AI model training. The initial dataset consisted of very high-resolution images with a pixel size of 0.3939 µm. The mean slide width and height were 83,621 and 46,123 pixels, respectively. The mean file size was 2.85 GB, and the total file size was 2,085 GB. Ethical approval was obtained from the Institutional Review Board of Hacettepe University (reference number: GO 21/1178, approval date: 05 April 2022). All methods were carried out in accordance with relevant guidelines and regulations.

Annotation of the images was performed in consensus by a senior dermatologist certified in Mohs micrographic surgery (G.E.) and a senior dermatopathologist (O.G.), who jointly reviewed the images and labeled the tumor regions (red) and artifact/non-tumor regions (green) using QuPath (version 0.4.2) [8], a digital pathology program. The complementary expertise of the two annotators supported the comprehensiveness and accuracy of the annotations.

For training of the deep learning model, 731 high-resolution annotated slides were cropped into smaller sizes to omit empty regions and increase model performance, yielding 91 tumor regions and 640 non-tumor regions. The dataset specifications are shown in Table 1. The slide resolution was downsampled by a factor of two before model training [9]. Experts (G.E. and O.G.) annotated tumor regions in red color and non-tumor regions in green color across the entire Mohs sections. After annotation, these areas were

Table 1 Dataset characteristics and patient-level split

Attribute	Total	Train	Val.	Test
Patients	51	36	8	7
Slides	731	536	103	92
Artifacts	640	472	91	77
Tumours	91	64	12	15

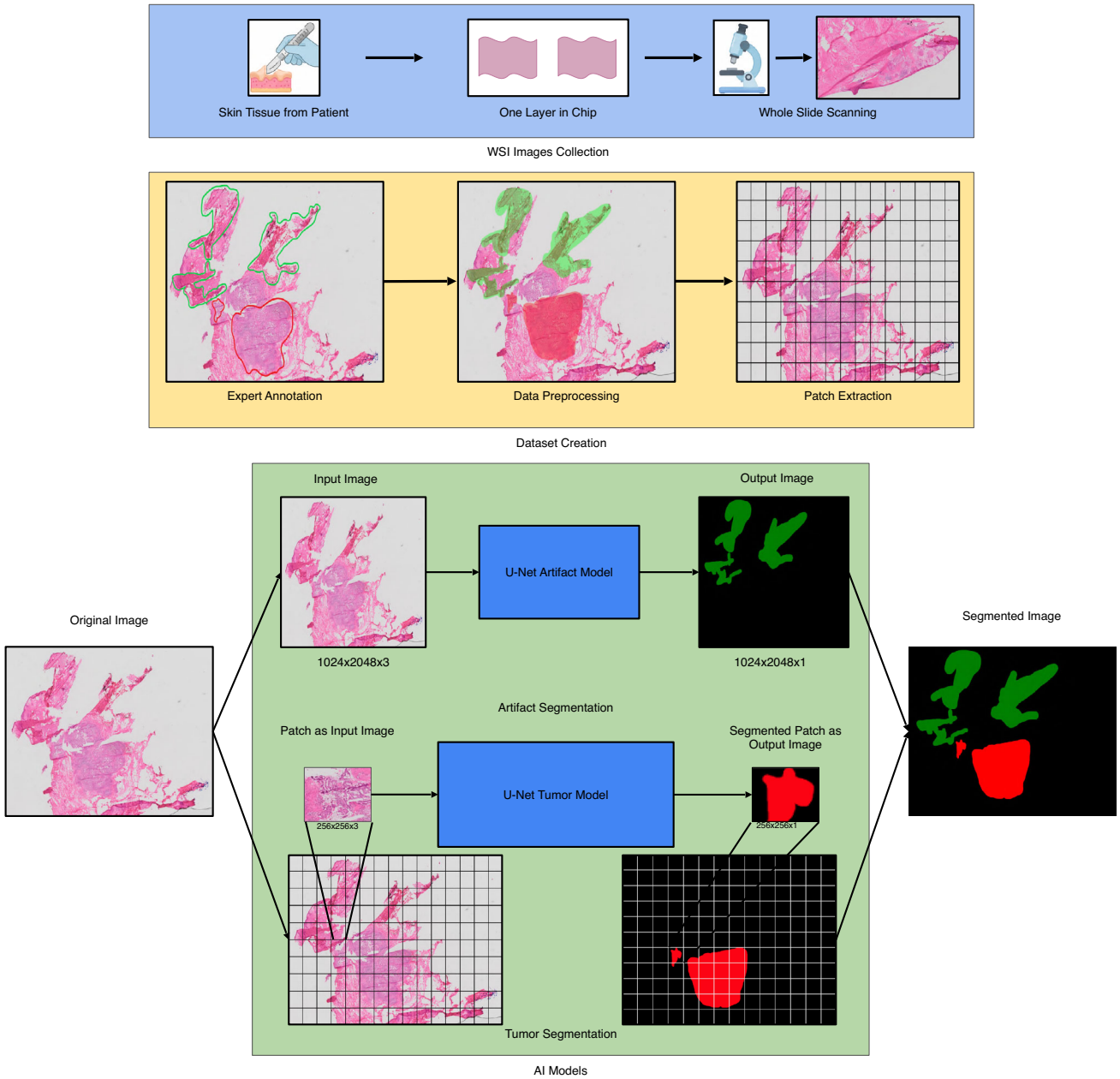


Fig. 1 The workflow for tumor segmentation on histopathology slides starts with collecting skin tissue from a patient, scanning it to obtain whole slide images (WSIs), and annotating the images by experts. The annotated images were preprocessed and the patches were extracted. A U-Net artifact detection model segments artifacts in the input images, and a U-Net tumor detection model further processes the patches to segment tumor regions. The final output is a segmented image highlighting tumor areas (red) and artifacts (green)

extracted and saved as mask images in separate .png files. The green channel was used to filter non-tumor regions, and the red channel was used to filter tumor regions. These filtered masks were then converted to grayscale and subsequently to binary images to reduce computational load. The non-tumor images were then resized to 1024 × 2048 pixels. Finally, the mask images and corresponding histopathology images were normalized to the range 0-1. These regions, along with their labels, were used as ground truth during training and validation of our deep learning model. To enhance the generalizability of the model and prevent overfitting, data augmentation techniques were applied to the patches using random rotations, horizontal and vertical flips, and zooms. An overview of the study is shown in Fig. 1.

2.1 Deep neural networks and model training

For an efficient segmentation of tumor and artifacts, we present a multi-model approach based on U-Net [10]. To detect tumors and non-tumor regions, we deployed two different U-Net architectures, a type of CNN designed specifically for image segmentation tasks. The architecture comprises an encoder that progressively reduces spatial dimensions while increasing the number of feature channels and a decoder that restores spatial resolution by combining high-level features with corresponding low-level encoder features through skip connections. The final layer of the U-Net model outputs a segmented image, where each pixel is assigned a class label (tumor or non-tumor region).

For model training, we used the capabilities of TensorFlow library (version 2.10) to facilitate a streamlined data processing workflow on Python programming language (version 3.9.5), which allowed us to efficiently manage the dataset. To prepare for model training and evaluation, we divided the labeled data into three sets: the training, validation, and test sets.The dataset was divided at the patient level into training, validation, and test sets, comprising 36, 8, and 7 patients, respectively, corresponding to approximately 70cohort. For segmentation models, ResNet-34 architecture which is pretrained on ImageNet dataset was used as a down-sampling part of U-Net architecture [11]. The segmentation models were optimized using Adam optimization algorithm with initial learning rate of 2e-4 and ReduceLROnPlateau approach that changes learning rate with its value of 0.2 when metrics do not increase for five epochs. The performance of the U-Net model was evaluated on a separate test dataset of image patches. Model training and optimization were performed on a workstation equipped with an NVIDIA GeForce RTX 3090 GPU, an Intel Core i7-11700KF CPU, and 128 GB of RAM. The first model segmented non-tumor regions. To preserve relevant structures while maintaining computational efficiency, all input images were resized to 1024 $\times$ 2048 pixels. This resizing approach was chosen to find a balance between maintaining essential anatomical details and avoiding computational bottlenecks.

For the tumor segmentation model, 256 $\times$ 256- pixel patches were extracted from the original images and corresponding masks. The original slide dimensions were otherwise preserved. This patch-based strategy retained fine-grained details while reducing the computational cost of analyzing large histopathology images. As part of the patch selection strategy, 256 $\times$ 256 patches were extracted from the whole-slide images. To reduce the predominance of empty or non-informative background regions, 80% of patches identified as non-tissue/background patches were randomly excluded during training and validation. This exclusion was not applied to expert-annotated tumor or artifact regions and was not intended to train a separate tissue detection model.

The main segmentation pipeline included two U-Net-based models: one trained for tumor segmentation and one trained for artifact/non-tumor region segmentation. These models were applied separately to identify their corresponding target regions. In addition to the segmentation models, we trained separate patch-level and slide-level tumor classification models for comparison. For patch-level classification, the same 256 $\times$ 256- pixel patches used for the tumor segmentation model were used to train a ResNet-101 architecture pretrained on ImageNet. For slidelevel classification, the whole-slide images were resized to 1024 $\times$ 2048 pixels and used to train a separate ResNet-101 architecture pretrained on ImageNet. These classification models were not combined with the segmentation models and were not part of the ensemble; they were used only to compare tumor classification performance at the patch and slide levels with the segmentation-based approach.

In addition to our custom non-tumor segmentation methods, we leveraged the nnUNet framework's capabilities. nnU-Net, a selfconfiguring method for deep learning-based biomedical image segmentation, proved to be a valuable component in our research pipeline. The nnU-Net framework, designed by Isensee et al. [12], operates as a versatile tool for automating the development of segmentation models in the context of medical imaging. By employing U-Net architecture as its base, nnU-Net dynamically adapts its architecture and hyperparameters based on the characteristics of the input data. This unique feature eliminates the need for laborious manual tuning, streamlining the process of model development.

2.2 Statistical analysis

To measure segmentation success, the Dice similarity coefficient and AUC score were calculated. The Dice coefficient is a quantitative statistic used to assess the degree of overlap between the predicted segmentation and the reference annotation. We also evaluated the performance of our model using the AUC score, which measures the model's ability to distinguish between positive and negative regions. An AUC score of 1 denotes perfect discrimination, whereas a score of 0.5 indicates performance no better than random chance. For patch-level classification, AUC was calculated using the standard binary classification approach based on the predicted tumor probability for each 256 $\times$ 256-pixel patch and its corresponding binary ground-truth label. The ground-truth patch label was assigned according to the corresponding tumor mask: a patch was considered tumor-positive when at least 10

Table 2 Performance metrics for the segmentation and classification models in tumor and artifact analysis

Type	Model	AUC Score	Dice Score
Tumor Segmentation	U-Net (ResNet-34)	0.98	0.70
Artifact Segmentation	nnU-Net	0.83	0.64
Artifact Segmentation	U-Net (ResNet-34)	0.96	0.67
Patch-Level Tumor Classification	ResNet-101	0.98	–
Slide-Level Tumor Classification	ResNet-101	0.91	–

3 Results & discussion

In this study, we present a multi-model deep learning system for tumor and artifact detection in MMS histopathological slides. We evaluated the performance of our U-Net-based deep learning models. Our approach demonstrated remarkable success, as quantified by the Dice score and AUC. The Dice score, a metric of overlap between the predicted and ground truth segmentation, was used to assess the performance of our model. In the test set evaluations, our model achieved Dice scores of 0.70 and 0.67 for tumor and non-tumor segmentation, respectively, alongside AUC scores of 0.98 and 0.96. These results indicate a high degree of overlap between the model's predictions and the ground truth. For comparison, the state-of-the-art AutoML segmentation method nnU-Net achieved a Dice score of 0.64 and an AUC of 0.83. These results underline the effectiveness of our model in accurately detecting tumor and non-tumor regions within histopathological images. For patch-level and slide-level tumor classification, our model achieved AUC scores of 0.98 and 0.91, respectively, on the test set. For patch-level BCC detection, sensitivity was 83.6% (95% CI, 79.5%–87.0%) and specificity was 97.3% (95% CI, 96.7%–97.9%). For slide-level BCC detection, sensitivity was 86.7% (95% CI, 62.1%–96.3%) and specificity was 84.4% (95% CI, 74.7%–90.9%). These scores indicate a high level of success in distinguishing tumor and artifact regions from healthy tissue and each other. The results are summarized in Table 2 and Figure 2.

Our study demonstrates the potential of a deep learning system to assist clinicians with the histopathological analysis of MMS slides. MMS is widely recognized as an effective treatment for high-risk BCCs and SCCs, with high reported cure rates [13]. MMS demonstrates excellent 5-year outcomes, with recurrence rates of 0

This growing burden on clinicians underscores the need for more widespread expertise in Mohs surgery. However, its training is conducted in a very limited number of centers and requires a long training period. Furthermore, the most significant challenge in this field is learning to accurately assess the tumor in pathology specimens rather than the surgical removal. In this context, the application of deep learning systems can be particularly transformative.

Addressing these challenges, AI can ensure that the evaluation process during surgery is conducted accurately and effectively. The results of our study suggest that Mohs surgeons may benefit from AI in challenging cases where there is uncertainty about the presence of a tumor. Incorrectly assessing non-tumor regions as tumors may lead to the unnecessary removal of healthy tissue, causing functional and cosmetic losses.

To improve the model's accuracy in detecting tumor regions, we trained the AI using high-magnification patches from digitized WSI of Mohs slides. This approach aligns with clinical workflows, where pathologists begin with a low magnification overview and then shift to high magnification for detailed examination. By focusing on high-magnification patches, the AI can better identify subtle morphological changes critical for distinguishing tumor cells from surrounding tissue. Additionally, a tissue detection algorithm was employed to automatically identify and isolate tissue-containing regions, enabling comprehensive slide analysis while minimizing time spent on non-informative areas. This combination of targeted training and efficient tissue detection enables the automated analysis of a Mohs WSI.

Our study supports the idea that training the AI model should be conducted not only for the tumor but also for potential non-tumor regions that can be confused with the tumoral area. The segmentation of non-tumor regions, including artifacts, can play a crucial role in enhancing the performance of AI models for histopathological image analysis. An ideal Mohs histopathological section should be free of artifacts such as fragmentation, folding, bubbles, or holes. However, real-life experience rarely allows perfectly ideal slides. To address this, we also trained our model on slides with pronounced artifacts that, while not meeting the quality assessment standards, were valuable for training the model to recognize artifacts. The inclusion of such slides and artifact segmentation as part of the multi-model approach aimed to strengthen the model's ability to distinguish between tumors and artifacts. In our study, we chose a full image training approach to detect non-tumor regions. This decision was based on the understanding that some non-tumor artifacts have more complex shapes, and preserving their spatial information is essential, which patching might compromise. The automatic detection of non-tumor artifacts can also be

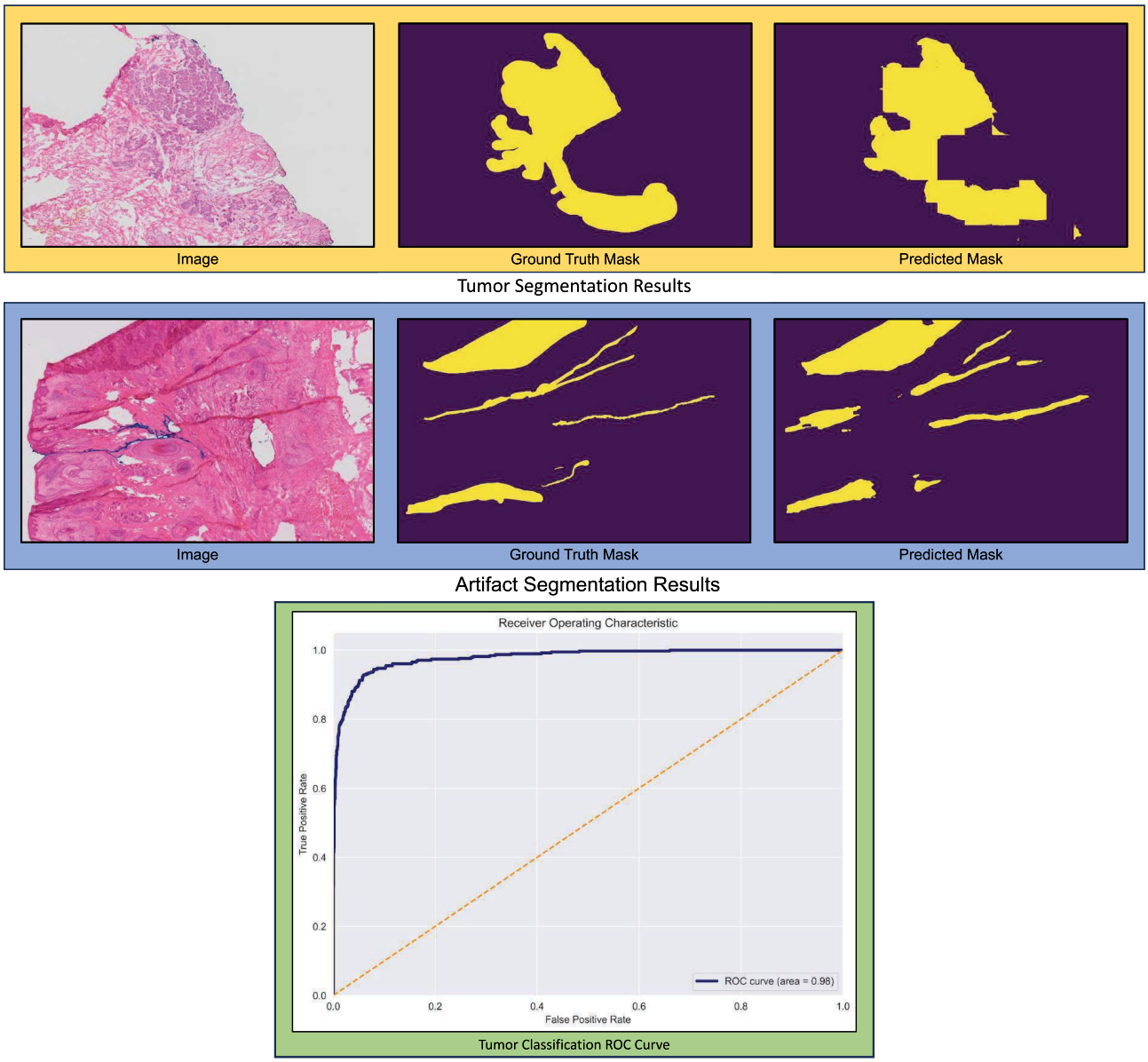


Fig. 2 Comparison of ground truth masks and predicted masks for tumor and artifact segmentation on Mohs slides. The top and middle rows display original images, corresponding ground truth masks, and predicted masks. The bottom panel shows the ROC curve for tumor classification, indicating a high area under the curve (AUC) of 0.98

part of a quality control system, ensuring the integrity of histopathological images. Such systems can potentially save examiners valuable time by alerting them to potential issues with a slide before they commence their analysis [17]. Furthermore, certain non-tumor artifacts might be mistaken for pathological features, leading to potential misinterpretations and incorrect diagnoses. Given that many machine learning algorithms are sensitive to these artifacts, their mismanagement can negatively affect the success of machine learning models if they are not correctly handled. In addition to non-tumor artifact detection, artifact annotation is also challenging because artifacts such as water droplets can occur on both tumor and healthy tissue. This situation increases the risk of false-positive and false-negative predictions during AI model training. Accurate annotation, detection, and segmentation of these artifacts are crucial for mitigating these risks. Moreover, this process can be used as examples during the training of residents and fellows to demonstrate common pitfalls and issues in slide preparation. Thus, while the primary focus in digital pathology often lies in the segmentation of biologically relevant features such as tumors, the iden-

tification of non-tumor artifacts is equally vital to develop successful AI systems for clinical practice.

There are significant opportunities for the application of AI in histopathology, which offers substantial potential. The automation of tasks traditionally performed by pathologists can improve diagnostic performance, reduce workload, and provide faster feedback during surgery [18]. This could, in turn, lead to reduced healthcare costs and improved patient outcomes [19]. Building on previous work, we developed a model for tumor and artifact detection in MMS slides. Zon et al. and Sohn et al. made important contributions to this field [6, 7]. More recently, Tan et al. proposed a tile-based classification model that generated probability-map overlays for Mohs-focused microscopic views and validated the model prospectively [20]. Our study distinguishes itself from prior works in several ways. We used two U-Net-based models for tumor and non-tumor-region segmentation and evaluated a ResNet-101 patch classifier. The internal test results showed promising discrimination, although external generalizability remains to be established.

Nevertheless, our study is not without limitations. First, the dataset was derived from a single center and included 731 whole-slide images obtained from 51 patients who underwent Mohs micrographic surgery performed by a single surgeon. Although the number of WSIs was relatively large, the limited number of patients, single-institution design, and single-surgeon source may limit the generalizability of our findings to other clinical settings, patient populations, tissue processing protocols, scanning systems, and surgical practices. Future studies should validate the proposed model using larger, multi-center datasets collected from multiple surgeons and institutions. Second, although annotations were produced by consensus between two experts, they may still be subject to observer-related variability. Future studies should include independent annotations from multiple experts followed by adjudication or consensus. In addition, although our model showed promising results, its clinical applicability needs to be validated through prospective studies in a real-world clinical setting. Future studies should specifically evaluate real-time deployment during Mohs surgery, including inference time, computational requirements, integration with digital slide scanning workflows, local or cloud-based processing strategies, and whether the model can provide timely and efficient decision support during surgical margin assessment.

Furthermore, although our model focused on BCC, future work could expand the training set to include other NMSCs, such as squamous cell carcinoma (SCC), to extend the model's applicability to additional tumor types. Additionally, due to the rarity of mimicker lesions and incidental malignancies in our dataset, our AI model was not specifically trained to differentiate BCC from benign entities commonly encountered during histopathological examination of Mohs slides (e.g., basaloid follicular hamartoma, granulomatous inflammation, syringoma) or incidental malignant lesions (e.g., atypical fibroxanthoma, sebaceous carcinoma, Merkel cell carcinoma) [21]. While this constitutes a limitation of our dataset and hence the resulting AI model, future studies could incorporate sufficient examples of these entities into their datasets to discriminate between BCC and its histopathologic mimickers.

4 Conclusion

Our study demonstrates the potential of a U-Net based model in histopathological image analysis for both tumor and non-tumor segmentation. This promising technology could have important impacts on pathology, transforming it from a predominantly manual practice to an automated one, enhanced by the precision and efficiency of AI. While considerable progress has been made, the field remains ripe for further exploration. Future research could investigate the identification and classification of additional skin cancers in telepathology settings. Deep learning decision-support systems could be developed to improve tumor-detection performance and accelerate slide analysis. In addition, future studies could evaluate and compare additional segmentation architectures beyond U-Net and nnU-Net to provide broader benchmarking and identify the most suitable models for Mohs histopathologic image analysis.

Acknowledgements None declared.

Author Contributions Conceptualization, A.Y., S.A.A., G.G., H.U., and G.E.; Methodology, A.Y., S.A.A., D.T., F.Y., B.D.K. and R.V.; Data Collection, S.A.A. and O.G.; Writing-Original Draft Preparation, A.Y., S.A.A., H.U. and G.E.; and A.Y. and R.V. prepared figures. All authors reviewed the manuscript.

Funding Abdurrahim Yilmaz has been funded by the President's PhD Scholarships at Imperial College London.

Data Availability The datasets used and/or analyzed during the current study are available from the corresponding author on reasonable request.

Declarations

Competing Interests The authors declare no competing interests.

Ethical Approval Ethical approval was obtained from the Institutional Review Board of Hacettepe University (reference number: GO 21/1178; approval date: 05 April 2022). Informed consent was waived due to the retrospective nature of the study and the use of fully de-identified data with no protected health information (PHI).

Open Access This article is licensed under a Creative Commons Attribution 4.0 International License, which permits use, sharing, adaptation, distribution and reproduction in any medium or format, as long as you give appropriate credit to the original author(s) and the source, provide a link to the Creative Commons licence, and indicate if changes were made. The images or other third party material

in this article are included in the article's Creative Commons licence, unless indicated otherwise in a credit line to the material. If material is not included in the article's Creative Commons licence and your intended use is not permitted by statutory regulation or exceeds the permitted use, you will need to obtain permission directly from the copyright holder. To view a copy of this licence, visit http://creativecommons.org/licenses/by/4.0/.

References

1. Cireşan, D.C., Giusti, A., Gambardella, L.M., Schmidhuber, J.: Mitosis Detection in Breast Cancer Histology Images with Deep Neural Networks. In: Mori, K., Sakuma, I., Sato, Y., Barillot, C., Navab, N. (eds.) Medical Image Computing and Computer-Assisted Intervention – MICCAI 2013, pp. 411–418. Springer, Berlin, Heidelberg (2013). https://doi.org/10.1007/978-3-642-40763-5_51
2. Litjens, G., Kooi, T., Bejnordi, B.E., Setio, A.A.A., Ciompi, F., Ghafoorian, M., Laak, J.A.W.M., Ginneken, B., Sánchez, C.I.: A survey on deep learning in medical image analysis. Med. Image Anal. **42**, 60–88 (2017). https://doi.org/10.1016/j.media.2017.07.005
3. Talo, M.: Automated classification of histopathology images using transfer learning. Artif. Intell. Med. **101**, 101743 (2019). https://doi.org/10.1016/j.artmed.2019.101743
4. Yilmaz, A., Gencoglan, G., Varol, R., Demircali, A.A., Keshavarz, M., Uvet, H.: MobileSkin: Classification of Skin Lesion Images Acquired Using Mobile Phone-Attached Hand-Held Dermoscopes. Journal of Clinical Medicine **11**(17) (2022) https://doi.org/10.3390/jcm11175102
5. Rivenson, Y., Wang, H., Wei, Z., Haan, K., Zhang, Y., Wu, Y., Günaydın, H., Zuckerman, J.E., Chong, T., Sisk, A.E., Westbrook, L.M., Wallace, W.D., Ozcan, A.: Virtual histological staining of unlabelled tissue-autofluorescence images via deep learning. Nat. Biomed. Eng. **3**(6), 466–477 (2019) https://doi.org/10.1038/s41551-019-0362-y
6. Zon, M.C., Waa, J.D., Veta, M., Krekels, G.A.: Whole-slide margin control through deep learning in mohs micrographic surgery for basal cell carcinoma. Exp. Dermatol. **30**(5), 733–738 (2021). http://doi.org/10.1111/exd.14306
7. Sohn, G.K., Sohn, J.H., Yeh, J., Chen, Y., Jiang, S.I.B. (2021). A deep learning algorithm to detect the presence of basal cell carcinoma on Mohs micrographic surgery frozen sections. J. American Acad. Dermatol. **84**(5), 1437–1438. https://doi.org/10.1016/j.jaad.2020.06.080
8. Bankhead, P., Loughrey, M.B., Fernández, J.A., Dombrowski, Y., McArt, D.G., Dunne, P.D., McQuaid, S., Gray, R.T., Murray, L.J., Coleman, H.G., James, J.A., Salto-Tellez, M., Hamilton, P.W.: QuPath: Open source software for digital pathology image analysis. Sci. Rep. **7**(1), 16878 (2017). https://doi.org/10.1038/s41598-017-17204-5
9. Boumaraf, S., Liu, X., Wan, Y., Zheng, Z., Ferkous, C., Ma, X., Li, Z., Bardou, D.: Conventional Machine Learning versus Deep Learning for Magnification Dependent Histopathological Breast Cancer Image Classification: A Comparative Study with Visual Explanation. Diagnostics **11**(3) (2021) https://doi.org/10.3390/diagnostics11030528
10. Ronneberger, O., Fischer, P., Brox, T.: U-Net: Convolutional Networks for Biomedical Image Segmentation. In: Navab, N., Hornegger, J., Wells, W.M., Frangi, A.F. (2015) Medical Image Computing and Computer-Assisted Intervention – MICCAI 2015, pp. 234–241. Springer, Cham. https://doi.org/10.1007/978-3-319-24574-4_28
11. He, K., Zhang, X., Ren, S., Sun, J.: Deep Residual Learning for Image Recognition. In: 2016 IEEE Conference on Computer Vision and Pattern Recognition (CVPR), Las Vegas, NV, USA, 2016, pp. 770–778, https://doi.org/10.1109/CVPR.2016.90
12. Isensee, F., Jaeger, P.F., Kohl, S.A., Petersen, J., Maier-Hein, K.H.: nnu-net: a self-configuring method for deep learning-based biomedical image segmentation. Nat. Methods **18**(2), 203–211 (2021). https://doi.org/10.1038/s41592-020-01008-z
13. Shriner, D.L., McCoy, D.K., Goldberg, D.J., Wagner, R.F.: Mohs micrographic surgery. J. Am. Acad. Dermatol. **39**(1), 79–97 (1998). https://doi.org/10.1016/s0190-9622(98)70405-0
14. Malhotra, R.: The Australian Mohs database, part II*1Periocular basal cell carcinoma outcome at 5-year follow-up. Ophthalmology **111**(4), 631–636 (2004). https://doi.org/10.1016/j.ophtha.2003.11.004
15. Malone, J.P., Fedok, F.G., Belchis, D.A., Maloney, M.E.: Basal cell carcinoma metastatic to the parotid: report of a new case and review of the literature. Ear, Nose & Throat J. **79**(7), 511–519 (2000)
16. Ciazynska, M., Slawinska, M., Kaminska-Winciorek, G., Lange, D., Lewandowski, B., Reich, A., Pabianek, M., Szczepaniak, K., Hankiewicz, A., Ulanska, M., et al.: Clinical and epidemiological analysis of basosquamous carcinoma: results of the multicenter study. Sci. Rep. 10(1), 18475 (2020). http://doi.org/10.1038/s41598-020-72732-x
17. Fourcade, A., Khonsari, R.H.: Deep learning in medical image analysis: A third eye for doctors. J. Stomatol. Oral Maxillofac. Surg. **120**(4), 279–288 (2019). https://doi.org/10.1016/j.jormas.2019.06.002
18. Cui, M., Zhang, D.Y.: Artificial intelligence and computational pathology. Lab. Invest. **101**(4), 412–422 (2021). https://doi.org/10.1038/s41374-020-00514-0
19. Homeyer, A., Lotz, J., Schwen, L.O., Weiss, N., Romberg, D., Höfener, H., Zerbe, N., Hufnagl, P.: Artificial Intelligence in Pathology: From Prototype to Product. J. Path. Inf. **12**, 13 (2021) https://doi.org/10.4103/jpi.jpi_84_20
20. Tan, E., Lim, S., Lamont, D., Epstein, R., Lim, D., Lin, F.P.Y.: Development and validation of a deep learning model for improving detection of nonmelanoma skin cancers treated with Mohs micrographic surgery. JAAD Int. **14**, 39–47 (2024). https://doi.org/10.1016/j.jdin.2023.10.007
21. Pousti, B.T., Brian Jiang, S.I., Darsha, A.K., Hau, J.T., Loh, T.Y. Removal of Incidental Skin Cancer During Mohs Micrographic Surgery Indicated for a Different Primary Tumor. Dermatol Surg. **50**(4), 327–330 (2024). https://doi.org/10.1097/DSS.0000000000004081

Publisher's Note Springer Nature remains neutral with regard to jurisdictional claims in published maps and institutional affiliations.